Propagation Measurement and Channel Characteristics of Small Office OAM Communication at 30 GHz

Yang Wang, *Senior Member, IEEE*, Zhejia Zhang, Xi Liao, *Senior Member, IEEE*, Yi Tian, Jihua Zhou, and Jie Zhang, *Senior Member, IEEE*

***Abstract*—Orbital angular momentum (OAM) communication has been envisioned as a potential technology to increase capacity for 6G communication. In this letter, we present an OAM channel measurement campaign in an indoor small office at 30 GHz. Furthermore, the path loss is investigated and modeled by close-in (CI) model and floating-intercept (FI) model. It is found that the FI model fits the measured path loss better than the CI model, and the CI model may no longer appropriate for OAM wave propagation when the receiver is in the hollow radiation area of the OAM beam. Also, we investigate the K-factor and the results indicate that the divergence angle leads to more complicated multipath propagation characteristics of the wireless channel. Moreover, root mean square delay spread reveals that channel performance can be effectively improved when the receiver is within the direct radiation range of the OAM antenna. Generally, this work can be considered as a foundation of understanding and building channel models of indoor OAM communication systems.**

***Index Terms*—Channel measurement, millimeter wave, orbital angular momentum (OAM), propagation characteristics.**

I. Introduction

ORBITAL angular momentum (OAM), as a physical quantity of electromagnetic wave, provides a new degree of freedom resource for 6G wireless communication system [1]. Vortex electromagnetic wave (also called OAM wave) carrying OAM can enormously improve spectrum efficiency at the millimeter-wave (mm-wave) band [2]. However, the propagation characteristics of OAM wave are different from traditional electromagnetic wave at mm-wave band. Since the helical phase fronts and hollow intensity distribution appear distortions when the OAM wave are reflected and refracted [3], and the channel characteristics are affected by the propagation distance and the receiver aperture size [2]. Accordingly, OAM wave are considered better for shorter-range communications [4]. Thus, it is essential to characterize the indoor propagation characteristics of OAM wave at mm-wave band.

Channel measurement is an important approach to investigating channel characteristics [5]. A number of channel measurement campaigns have recently concentrated on common mm-wave bands, such as 28, 38, 60, and 73 GHz in indoor scenarios based on traditional mm-wave antenna [6], [7], [8], [9]. However, there are fewer channel measurements that focus on OAM wave.

The current research works of OAM wave propagation were mainly based on numerical simulations [10], [11], [12], [13], [14] and fewer actual measurements [15], [16], [17]. On the one hand, numerous research works have been carried out to investigate the effect of atmospheric turbulence [11] and multipath [12], [13], [14] on vortex wave propagation characteristics through simulations. For instance, a sparse multipath environment was constructed to investigate a hybrid orthogonal division multiplexing scheme for improving wireless channel capacity in [10]. On the other hand, some measurement campaigns were also conducted in some environments, e.g., open roofs, conference rooms, corridors [15], [16], [17]. In [15], the planar spiral OAM wave-based multiple-input–multiple-output (MIMO) system was used to investigate channel characteristics in line-of-sight (LOS) scenario, where the transmitter and receiver were 50 m apart, the result proved the possibility of OAM communication for wireless backhaul links. The author in [16] conducted an indoor measurement campaign at 5.8 GHz, then analyzed the received power and signal-to-noise ratio, the results indicated that the two conditions, alignment of antennas and suppression of reflections, were required for improving channel capacity with OAM antennas. In [17], an OAM misaligned channel characteristics was investigated in an indoor corridor environment at 3.5 GHz, it was found that the received power degraded as the increasing of misaligned angle. Up to now, the research works of OAM wave propagation characteristics are not comprehensive, especially indoor channel measurements are less at mm-wave band.

To this end, this letter conducts an indoor channel measurement campaign with the aim of investigating the OAM channel propagation characteristics in an indoor environment at 30 GHz. The main contributions of this letter are as follows.

1) We choose an indoor office as the measurement environment and carry out OAM mm-wave channel measurement

Manuscript received 10 November 2022; revised 29 November 2022; accepted 29 November 2022. Date of publication 5 December 2022; date of current version 7 April 2023. This work was supported in part by the National Natural Science Foundation of China under Grant 62171071 and Grant 62271095; and in part by the Natural Science Foundation of Chongqing under Grant cstc2021jcyj-msxmX0634. *(Corresponding author: Xi Liao.)*

Yang Wang, Zhejia Zhang, Xi Liao, and Yi Tian are with the School of Communication and Information Engineering, and Chongqing Key Laboratory of Complex Environmental Communications, Chongqing University of Posts and Telecommunications, Chongqing 400065, China (e-mail: wangyang@cqupt.edu.cn; s200131245@stu.cqupt.edu.cn; liaoxi@cqupt.edu.cn; s200101092@stu.cqupt.edu.cn).

Jihua Zhou is with the Aerospace New Generation Communications Company Ltd., Chongqing 401332, China (e-mail: jhzhou@ict.ac.cn).

Jie Zhang is with the Department of Electronic and Electrical Engineering, University of Sheffield, Sheffield S10 2TN, U.K. (e-mail: zhangjie123@cqupt.edu.cn).

Digital Object Identifier 10.1109/LAWP.2022.3226469

campaign at 30 GHz. Then, to compare the propagation characteristics of OAM waves, a pair of OAM antennas based on spiral phase plates (SPP) are employed at the receiver and transmitter as the case of OAM wave propagation. In addition, two other Tx–Rx systems cases are presented as references: the traditional mm-wave horn antennas, and the OAM antenna with a lens.

2) We build the path loss model for OAM wave propagation at 30 GHz based on measured data. Also, the propagation characteristics of OAM wave are analyzed, such as K-factors and root mean square (RMS) delay spread. This letter provides insights into the future deployment of indoor mm-wave OAM communication.

The rest of this letter is organized as follows. Section II describes the channel characteristics. Section III introduces the channel measurement campaign, including the measurement platform, environment, and deployment. In Section IV, the path loss models are obtained and the channel characteristics are analyzed. Finally, Section V concludes this letter.

II. Channel Characteristics

Based on the measured data, several research methods are introduced to shed light on indoor OAM channel characteristics, in terms of path loss, Rician K-factor, and delay spread in the mm-wave band.

A. Path Loss

Path loss is the amount of loss introduced by the propagation environment between the transmitter and receiver. Then, the path loss model is used to characterize the power attenuation as a function of transmission distance in a specific scenario.

First, we get the channel impulse response (CIR) $h(\tau, \theta_i)$, and then the omnidirectional received power $P(\tau_l)$ can be synthesized by each received power at a different angle [7], and the path loss can be written as

$$P(\tau_l) = \sum_{i=1}^{M} |h(\tau, \theta_i)|^2 \tag{1}$$

$$\mathrm{PL[dB]} = P_{\mathrm{tx}} - 10\lg\left[\sum_{l=1}^{L} P(\tau_l)\right] + G_{\mathrm{LNA}} + G_{\mathrm{rx}} + G_{\mathrm{tx}} - L_{\mathrm{other}} \tag{2}$$

where $h(\tau, \theta_i)$ denotes the CIR with the receiving angle θ_i and delay τ, M is the number of rotation steps, L means the number of multipaths, $P(\tau_l)$ is the reveived power in the τ_lth delay, P_{tx}, G_{LNA}, G_{rx}, G_{tx}, and L_{other} represent transmitted power, low noise amplifier (LNA) gain, transmitting antenna gain and receiving antenna gain, and other losses, respectively. Noted that the received power contains noise, only the signals above the noise threshold are considered [18].

The close-in (CI) model and floating-intercept (FI) model are represented as [7]

$$\mathrm{PL_{CI}}(d) = L_{\mathrm{path}}(d_0) + 10n\lg\left(\frac{d}{d_0}\right) + X_\sigma \tag{3}$$

$$\mathrm{PL_{FI}}(d) = \alpha + 10\beta\lg\left(\frac{d}{d_0}\right) + X_\sigma \tag{4}$$

where $L_{\mathrm{path}}(d_0)$ is the free space path loss at the reference distance $d_0 = 1$ m, n is the path loss exponent, X_σ denotes a normally distributed random varible with a standard deviation of σ in dB. In the FI model, α and β are the FI and the slope of model, respectively.

B. Rician K-Factor

The Rician K-factor is defined as the ratio of the dominant component power to the other multipath components. It can be expressed as

$$\mathrm{KF} = \frac{P_d}{\sum_{l=1}^{L} P(\tau_l) - P_d} \tag{5}$$

where P_d represent the power of dominant path, $\sum_{l=1}^{L} P(\tau_l)$ denote total power of all paths.

C. Delay Spread Characteristics

Power delay profile (PDP) describes the received power as a function of time delay. Also, delay spread is a metric of the multipath richness of communication channel. The parameters including mean arrival delay and rms delay spread can be derived from the PDP, and characterize the delay dispersion characteristics [7]. RMS delay spread can be given by

$$\tau_{\mathrm{rms}} = \sqrt{\frac{\sum_{l=1}^{L} (\tau_l - \tau_{\mathrm{mean}})^2 P(\tau_l)}{\sum_{l=1}^{L} P(\tau_l)}} \tag{6}$$

where the mean arrival delay is calculated as

$$\tau_{\mathrm{mean}} = \frac{\sum_{l=1}^{L} \tau_l P(\tau_l)}{\sum_{l=1}^{L} P(\tau_l)}. \tag{7}$$

III. Measurement Campaign

In this section, we conduct a small office OAM channel measurement campaign at 30 GHz based on a vector network analyzer (VNA). In the following, we would introduce the measurement platform, measurement environment, and measurement deployment.

A. Measurement Platform

The OAM channel measurement platform at 30 GHz consists of a VNA, the OAM antennas at both Tx and Rx sites based on SPP, an LNA with the gain of 35 dB, and a programmable pan-tilt-zoom (PTZ) rotator. For VNA, the measured bandwidth is 6 GHz, therefore, the delay domain resolution is 0.1667 ns, and the bandwidth of intermediate frequency (IF) bandpass filter is set to 1 kHz and the transmitted power is set to 0 dBm. Simultaneously, the frequency sweep points are 601, and the maximum excess delay is calculated as 100 ns, accordingly the maximum detection distance is 30 m. In addition, the OAM antenna consists of a standard gain horn antenna and an SPP with mode $l = 1$ [19], and the measured divergence angle is 11°, noted that the hollow amplitude distribution of the SPP-based OAM antenna performs properly at 27–33 GHz, which is proved in an anechoic chamber as shown in Fig. 1. Moreover, the half power beam width (HPBW) of the Rx horn antenna is 54.2°, therefore, the PTZ control the receiving azimuth angles Θ ($\Theta = [0°, 60°, 120°, 180°, 240°, 300°]$) at the Rx site, and the number of rotation steps $M = 6$. The experimental parameters are listed in Table I.

B. Measurement Environment and Measurement Deployment

We carry out the channel measurement campaign in a typical small office with an area of 9 m × 3.2 m and a ceiling height of 3.1 m. Also, the office is furnished with desks, chairs, printers,

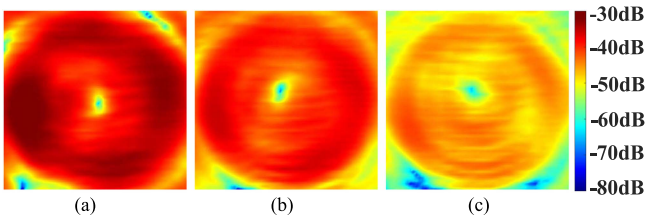

Fig. 1. Amplitude distribution of OAM antenna. (a) 27 GHz. (b) 30 GHz. (c) 33 GHz.

TABLE I
MEASUREMENT PARAMETERS

Parameter	Value
Measurement frequency	27-33 GHz
Sweep point	601
IF bandwidth	1 kHz
Transmitted power	0 dBm
Received angle	[0°, 60°, 120°, 180°, 240°, 300°]
LNA gain	35 dB
Tx horn antenna gain	20 dBi
Tx horn antenna HPBW	15.6°
Rx horn antenna gain	10 dBi
Rx horn antenna HPBW	54.2°
SPP & Lens loss	3 dB & 2 dB

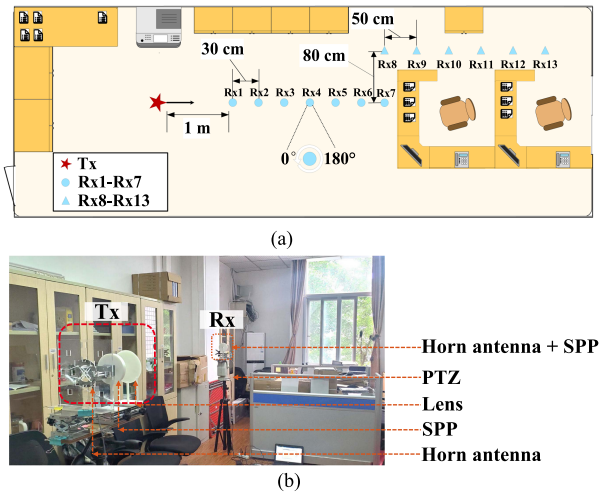

Fig. 2. (a) Deployment of channel measurement. (b) Photograph of the office environment.

bookshelves, etc. The detailed placement of the office furniture can be seen in Fig. 2.

In our measurement deployment, Tx is located at the red pentagram and the propagation direction is fixed. Then, 13 Rx positions in the far-field region of the Tx antenna are set in the office, with the initial receiving angle of 0° at each position, as depicted in the top view of the office in Fig. 2(a). Additionally, it can be seen that Rx1–Rx7 are in the pointing direction of Tx, however, Rx8–Rx13 are offset by 80 cm and are in the coverage area of the diverging OAM beam.

We investigate three Tx–Rx systems, as shown in Table II. *Case 1*: the transmitter and receiver are standard gain horn antennas to radiate the traditional mm-wave as a reference. *Case 2*: the SPPs are added in front of horn antennas, OAM wave can be generated. *Case 3*: an additional lens is employed in front of the SPP at Tx, which is designed to reduce the divergence angle and converge the OAM beam [19].

TABLE II
ANTENNA SYSTEM CASE

Case	Tx	Rx
Case 1	Tx horn antenna	Rx horn antenna
Case 2	Tx horn antenna+SPP	Rx horn antenna+SPP
Case 3	Tx horn antenna+SPP+Lens	Rx horn antenna+SPP

TABLE III
CI AND FI MODEL FITTING RESULT

			CI Model		FI Model		
	Case	$\mathrm{PL_{avg}}$/dB	n	σ/dB	α	β	σ/dB
Rx1-7	1	75.81	4.70	3.51	69.28	2.56	5.38
	2	97.63	10.77	15.28	94.53	1.21	2.69
	3	82.45	6.46	7.51	77.80	1.85	3.98
Rx8-13	1	91.82	4.85	3.08	79.93	1.96	2.75
	2	87.75	4.17	3.58	83.56	0.69	1.33
	3	90.91	4.61	7.05	105.39	-2.38	3.36

IV. RESULTS AND ANALYSIS

This section presents the path loss using both the CI model and the FI model. Then, K-factors are used to analyze the multipath richness of channel. Also, the time domain dispersion characteristic is investigated with rms delay spread.

A. Path Loss

Table III shows least-squares fits calculated for the parameters in the CI and FI models. For the receiver located at Rx1–Rx7, the average path loss $\mathrm{PL_{avg}}$ in case 2 and 3 is 97.63 dB and 82.45 dB, respectively, both of which are higher than the average path loss of 75.81 dB in case 1. This result reveals that the path loss in the Tx antenna pointing direction increases due to the beam divergence.

Fig. 3 shows measured results and fitted CI and FI models for the three cases. Rappaport et al. [7] concluded that the CI model should be used in preference to the FI model as it has a clear physical basis that depends on the working frequency and the reference distance $d_0 = 1$ m. However, this may not apply to OAM waves as demonstrated in Fig. 3(b), where the FI model is a much better fit than the CI model. Because of the divergence angle, Rx1–Rx7 are in the hollow radiation region and not directly pointed by the OAM beam.

When the receiver is located in the Rx8–Rx13, the average path loss is 87.75 dB in case 2, it becomes the minimum among three cases. This is probably because the receivers are in the direct radiation region of the OAM beam. Similarly, as a result of the narrowing of the OAM beam in case 3, the direct radiation area can reach farther locations, and the path loss decreases at Rx11–Rx13. Furthermore, the CI model fitting result is similar to the FI model in case 2, indicating that the CI model would be suitable for OAM wave propagation when the receiver is within the radiation area of the OAM beam.

B. Rician K Factor

The cumulative distribution function (CDF) of the K-factor for the three cases is shown in Fig. 4. On the one hand, it can be seen that more than 80% of the K-factors in case 2 are less than 0 dB from Fig. 2(a), which means that the other multipath components are larger than the dominant path when the Rx is placed in the direction of antenna pointing. This may result from the divergence angle, the OAM beam is more likely to

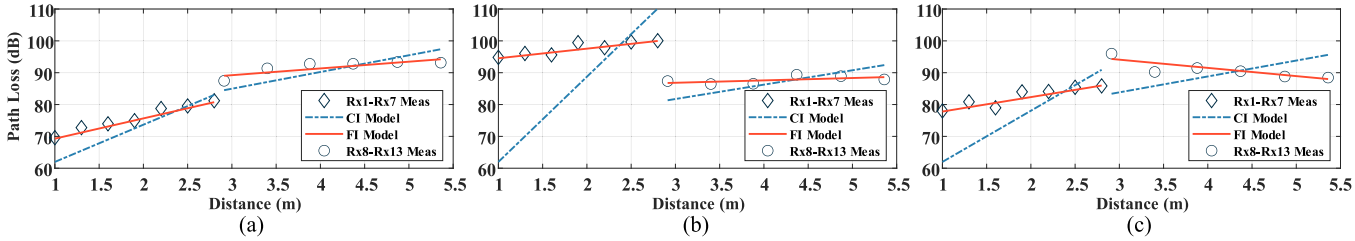

Fig. 3. Path loss. (a) Case 1. (b) Case 2. (c) Case 3.

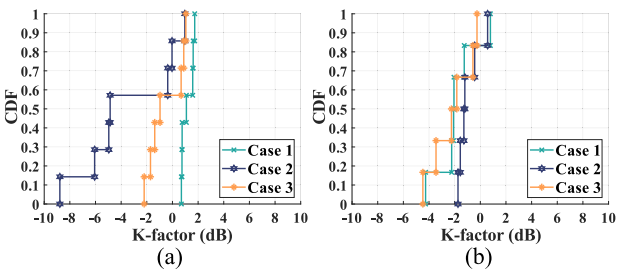

Fig. 4. CDF of K-factors. (a) Rx1–Rx7. (b) Rx8–Rx13.

TABLE IV
MEAN K-FACTORS

	Case 1	Case 2	Case 3
Rx1-Rx7	1.17	-3.44	-0.52
Rx8-Rx13	-1.85	-0.94	-2.14

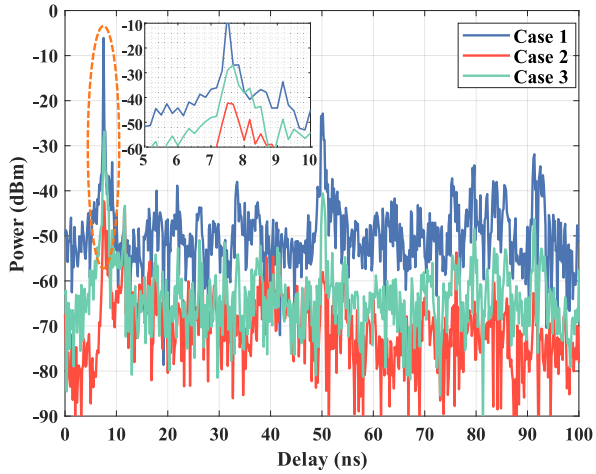

Fig. 5. PDP at Rx4.

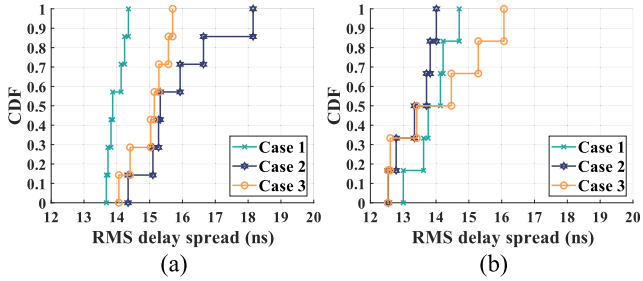

Fig. 6. CDF of rms delay spread. (a) Rx1–Rx7. (b) Rx8–Rx13.

be affected by indoor scatterers, such as walls and floors. Also, decreasing the divergence angle can help mitigate these impacts as demonstrated in case 3.

On the other hand, it can be seen that the mean K-factor increases to −0.94 dB in case 2 when the Rx is located at Rx8–Rx13 from Table IV. This means that the power of the dominant path has increased, or the power of the other multipath components has decreased, or both. In short, the divergence angle causes the channel multipath propagation characteristics to become complicated. Thus, the pattern of OAM beam and divergence angle should be considered when deploying receivers in OAM communication systems.

C. Delay Spread

Fig. 5 shows the PDP at the Rx4 position for the three cases, showing a decrease of the received power in the dominant path for the OAM cases, worst for case 2. Furthermore, the other multipath components are strongly attenuated for case 2, and the noise level is approximately the same as case 3. This is because that the received power of the first path is less when Rx is located in the hollow radiation area for case 2, whereas other multipaths are affected by reflections and other propagation mechanisms, therefore, the received power is attenuated.

Fig. 6 shows the CDF of the rms delay spread. For Rx1–Rx7 positions in Fig. 6(a), we see that the rms delay spread worsens for the OAM cases. This is a consequence of beam divergence. The situation improves significantly in case 3 when the divergence angle is reduced. For the Rx8–Rx13 positions in Fig. 6(b), the OAM system in case 2 performs better than the classical antenna system in case 1 in the direct radiation region of the OAM beam, but the reduced divergence beam in case 3 performs worse. These results demonstrate the complexity of OAM channel analysis.

V. CONCLUSION

In this letter, an indoor mm-wave OAM channel measurement campaign is conducted, and the path loss, K-factor, and rms delay spread are investigated to characterize OAM wave propagation characteristics. The results demonstrate that the CI model is inapplicable to OAM wave propagation when the receiver is outside the direct radiation region of the OAM beam, and channel characteristics and multipath richness can be enhanced by divergence angle in the office scenario. In addition, a lens can be used to suppress the OAM beam, the results reveal that OAM wave with smaller divergence angle is more resistant to multipath interference. Therefore, the deployment location of receiver and a small divergence angle are key factors that should be taken into consideration when OAM communication systems are deployed.

REFERENCES

[1] Z. Zhang et al., "6G wireless networks: Vision, requirements, architecture, and key technologies," *IEEE Veh. Technol. Mag.*, vol. 14, no. 3, pp. 28–41, Sep. 2019.

[2] Y. Yan et al., "High-capacity millimetre-wave communications with orbital angular momentum multiplexing," *Nature Commun.*, vol. 5, no. 1, pp. 48–76, Sep. 2014.

[3] Y. Yao, X. Liang, M. Zhu, J. Geng, and R. Jin, "Analysis and experiments on reflection and refraction of orbital angular momentum waves," *IEEE Trans. Antennas Propag.*, vol. 67, no. 4, pp. 2085–2094, Apr. 2019.

[4] D. K. Nguyen et al., "Antenna gain and link budget for waves carrying orbital angular momentum," *Radio Sci.*, vol. 50, no. 11, pp. 1165–1175, Nov. 2015.

[5] I. A. Hemadeh, K. Satyanarayana, M. El-Hajjar, and L. Hanzo, "Millimeter-wave communications: Physical channel models, design considerations, antenna constructions, and link-budget," *IEEE Commun. Surveys Tut.*, vol. 20, no. 2, pp. 870–913, Apr.–Jun 2018.

[6] A. Al-Saman et al., "Survey of millimeter-wave propagation measurements and models in indoor environments," *Electronics*, vol. 10, no. 14, pp. 1653, Jul. 2021.

[7] T. S. Rappaport, G. R. MacCartney, M. K. Samimi, and S. Sun, "Wideband millimeter-wave propagation measurements and channel models for future wireless communication system design," *IEEE Trans. Commun.*, vol. 63, no. 9, pp. 3029–3056, Sep. 2015.

[8] A. Bamba, F. Mani, and R. D'Errico, "Millimeter-wave indoor channel characteristics in *V* and *E* bands," *IEEE Trans. Antennas Propag.*, vol. 66, no. 10, pp. 5409–5424, Oct. 2018.

[9] P. Zhang, J. Li, H. Wang, and W. Hong, "Indoor small-scale spatiotemporal propagation characteristics at multiple millimeter-wave bands," *IEEE Antennas Wireless Propag. Lett.*, vol. 17, no. 12, pp. 2250–2254, Dec. 2018.

[10] L. Liang, W. Cheng, W. Zhang, and H. Zhang, "Joint OAM multiplexing and OFDM in sparse multipath environments," *IEEE Trans. Veh. Technol.*, vol. 69, no. 4, pp. 3864–3878, Apr. 2020.

[11] H. Lou, X. Ge, and Q. Li, "The new purity and capacity models for the OAM-mmwave communication systems under atmospheric turbulence," *IEEE Access.*, vol. 7, pp. 129988–129996, 2019.

[12] X. Chen and W. Xue, "OAM multiplexing in multipath environment," in *Proc. IEEE MTT-S Int. Conf. Numer. Electromagn. Multiphys. Model. Optim.*, Hangzhou, China, 2020, pp. 1–4.

[13] W. Xue et al., "A revisit of orbital angular momentum multiplexing in multipath environment," *J. Commun. Inf. Netw.*, vol. 5, no. 4, pp. 438–446, Dec. 2020.

[14] W. Jie et al., "Propagation model for UCA-based OAM communications in six-ray canyon channels," in *Proc. 14th Eur. Conf. Antennas Propag.*, Copenhagen, Denmark, 2020, pp. 1–4.

[15] X. Xiong et al., "Experimental study of plane spiral OAM mode-group based MIMO communications," *IEEE Trans. Antennas Propag.*, vol. 70, no. 1, pp. 641–653, Jan. 2022.

[16] B. Jeong, H. Kim, and H. Lee, "Indoor propagation of electromagnetic waves with orbital angular momentum at 5.8 GHz," *Int. J. Antennas Propag.*, vol. 2018, 2018, Art. no. 5634826.

[17] Y. Wang, P. Shi, X. Liao, T. Hu, J. Zhang, and A. Tennant, "Measurements of 3.5 GHz OAM misaligned channels in indoor corridor scenarios," *Proc. IEEE Int. Symp. Antennas Propag. USNC-URSI Radio Sci. Meeting*, Singapore, 2021, pp. 235–236.

[18] P. Zhang, J. Li, H. Wang, and X. You, "Millimeter-wave space-time propagation characteristics in urban macrocell scenarios," in *Proc. IEEE Int. Conf. Commun.*, Shanghai, China, 2019, pp. 1–6.

[19] B. Allen et al., "Experimental evaluation of 3D printed spiral phase plates for enabling an orbital angular momentum multiplexed radio system," *Roy. Soc. Open Sci.*, vol. 6, Dec. 2018, Art. no. 191419.